Journal Pre-proof

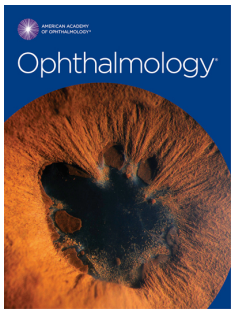

Autosomal recessive bestrophinopathy: clinical features, natural history and genetic findings in preparation for clinical trials

Giuseppe Casalino, MD, FEBO, Kamron N. Khan, PhD, FRCOphth, Monica Armengol, Genevieve Wright, MSc, Nikolas Pontikos, PhD, Michalis Georgiou, MD, PhD, Andrew R. Webster, MD, FRCOphth, Anthony G. Robson, PhD, Parampal S. Grewal, MD, FRCSC, Michel Michaelides, MD, FRCOphth.

PII: S0161-6420(20)30978-7

DOI: https://doi.org/10.1016/j.ophtha.2020.10.006

Reference: OPHTHA 11507

To appear in: *Ophthalmology*

Received Date: 22 June 2020

Revised Date: 11 September 2020

Accepted Date: 2 October 2020

Please cite this article as: Casalino G, Khan KN, Armengol M, Wright G, Pontikos N, Georgiou M, Webster AR, Robson AG, Grewal PS, Michaelides M, Autosomal recessive bestrophinopathy: clinical features, natural history and genetic findings in preparation for clinical trials, *Ophthalmology* (2020), doi: https://doi.org/10.1016/j.ophtha.2020.10.006.

Autosomal recessive bestrophinopathy: clinical features, natural history and genetic findings in preparation for clinical trials

Giuseppe Casalino* MD, FEBO,[1,2] Kamron N. Khan* PhD, FRCOphth,[3] Monica Armengol,[4] Genevieve Wright MSc,[1] Nikolas Pontikos PhD,[1] Michalis Georgiou MD, PhD,[1] Andrew R Webster MD, FRCOphth,[1] Anthony G Robson PhD,[1] Parampal S. Grewal MD, FRCSC,[1] Michel Michaelides MD, FRCOphth.[1]

1 Moorfields Eye Hospital NHS Foundation Trust, London, UK and UCL Institute of Ophthalmology, University College London, London, UK
2 Oftalmico Hospital, ASST Fatebenefratelli Sacco, Milan, Italy
3 Leeds Teaching Hospitals NHS Trust, Leeds, UK
4 Guy's and St. Thomas' Hospital NHS Foundation Trust, London, UK

* These authors contributed equally to this work and so should be considered joint first authors

Correspondence Author:

Professor Michel Michaelides
UCL, Institute of Ophthalmology
11 – 43 Bath Street, London
EC1V 9EL, UK
michel.michaelides@ucl.ac.uk

Running Head: Clinical spectrum of ARB

Keywords: autosomal recessive bestrophinopathy, BEST1, retinal imaging, electrophysiology, genetics, and gene therapy.

Conflict of interests: No conflicting relationship exists for any author.

Financial support: Supported by grants from the National Institute for Health Research Biomedical Research Centre at Moorfields Eye Hospital NHS Foundation Trust and UCL Institute of Ophthalmology, The Wellcome Trust (099173/Z/12/Z), Moorfields Eye Charity, Retina UK, and the Foundation Fighting Blindness (USA).

Meeting presentation: This study has been submitted for consideration for the upcoming American Academy of Ophthalmology Annual Meeting.

Abbreviations: ADB = autosomal dominant Best disease; ARB = autosomal recessive bestrophinopathy; CFP = color fundus photography; CNV = choroidal neovascularization; CRT = central retinal thickness; DA = dark adapted; DT = dark trough; EOG = electrooculogram; ERG = electroretinography; FAF = fundus autofluorescence; FCE = focal choroidal excavation; IRD = inherited retinal disease; LA = light adapted; LogMAR = logarithm of the minimum angle of resolution; LP = light peak; NIR = near infrared; OCT = optical coherence tomography; ORL = outer retinal layer; PED = pigment epithelial detachment; RPE = retinal pigment epithelium; SD = subretinal deposit; subretinal hyperreflective material = SHRM; SRF = subretinal fluid; VA = visual acuity.

ABSTRACT

Purpose: To investigate the clinical course, genetic findings and the phenotypic spectrum of autosomal recessive bestrophinopathy (ARB) in a large cohort of children and adults.

Design: Retrospective case series.

Participants: Patients with a detailed clinical phenotype consistent with ARB and/or biallelic likely disease-causing sequence variants in the *BEST1* gene, identified at a single tertiary referral center.

Methods: Review of case notes, retinal imaging (color fundus photography, fundus autofluorescence [FAF], optical coherence tomography [OCT]), electrophysiologic assessment, and molecular genetic testing.

Main Outcome Measures: Visual acuity (VA), retinal imaging and electrophysiologic changes over time.

Results: 56 eyes of 28 unrelated patients were included. Compound heterozygous variants were detected in the majority of patients (19/27), with six alleles recurring in apparently unrelated individuals, the most common of which was c.422G>A, p.(Arg141His), (n = 4 patients). Mean presenting VA was 0.52 ± 0.36 LogMAR and final VA was 0.81 ± 0.75 LogMAR ($p = 0.06$). The mean rate of change in VA was 0.05 ± 0.13 LogMAR/year. A significant change in VA was detected in patients with a follow-up ≥ 5 years (n = 18) compared to patients with a follow-up ≤ 5 years (n = 10, $p = 0.001$). Presence of subretinal fluid and vitelliform material were early findings in the majority of subjects and this did not substantially change over time. A reduction in central retinal thickness was detected in the majority of eyes (80.4%) over the course of follow-up. Many subjects (10/26) showed evidence of generalised rod and cone system dysfunction. These patients were older ($p < 0.001$) and had worse VA ($p = 0.02$), than those with normal full-field electroretinography.

Conclusions: Although patients with ARB are presumed to have no functioning bestrophin channels, significant phenotypic heterogeneity is evident. The clinical course is characterized by a progressive loss of vision, with a slow rate of decline, providing a wide therapeutic window for anticipated future treatment strategies.

The bestrophinopathies are a spectrum of inherited retinal dystrophies caused by pathogenic variation in the Bestrophin1 protein, encoded by the *BEST1* gene.[1,2] The gene product is a pentameric calcium-sensitive chloride channel which localises to the basolateral plasma membrane of the retinal pigment epithelium (RPE).[2–4] The channel regulates the flow of chloride and other anions based on intracellular calcium concentrations. Recent studies have improved our understanding of the architecture and function of this channel; there is a central ion pore and calcium dependent gating apparatus. Pathogenic mutations are prevalent in the gating apparatus.[5,6]

A wide array of unique *BEST1* variants have been reported, advancing our understanding of how genotypes influence phenotypes. The most prevalent variants are transmitted in an autosomal dominant pattern and are found in the first half of the gene, predicted to result in heterozygous missense variants.[1,2] *BEST1* haploinsufficiency appears to be tolerated, suggesting that dominant mutations act by conferring a gain-of-function effect; however this remains controversial.[7] Phenotypes associated with heterozygous pathogenic variants include: (1) conditions that predominantly affect the macula - Best disease (OMIM #153700) and adult vitelliform macular dystrophy (OMIM 153840); (2) those with generalized retinal involvement - autosomal dominant vitreoretinochoroidopathy and rod-cone dystrophy; and (3) diseases with retinal and anterior segment involvement - autosomal dominant microcornea, rod-cone dystrophy, early onset cataract, and posterior staphyloma.[1]

In 2006 Schatz et al. were the first to report two related patients harboring compound *BEST1* heterozygous variants and presenting with a multifocal vitelliform dystrophy.[8] Two years later, Burgess et al.[9] concluded that this condition was a fourth *BEST1*-associated phenotype, and coined the term autosomal recessive bestrophinopathy (ARB). The clinical features of ARB include multifocal vitelliform deposits and irregularity of the RPE - evident as hyper and hypo-autofluorescent areas at the posterior pole (Figure 1), intraretinal fluid, hypermetropia, and, in some, shallow anterior chambers, predisposing to angle closure glaucoma.[9] The EOG light peak to dark trough ratio is usually severely reduced due to severe generalised RPE dysfunction. Full-field electroretinography (ERG) is typically abnormal from late childhood or adolescence and indicates generalised rod and cone dysfunction,

however this is insufficient to explain the severe EOG reduction. In addition, there is pattern ERG evidence of macular dysfunction.[9]

Currently there is considerable interest in developing therapy for patients with inherited retinal disease, with gene replacement being the most advanced strategy at present. Voretigene neparvovec-rzyl (Luxturna) is already available for the treatment of biallelic *RPE65*-associated retinal dystrophy, with further trials underway to treat *CHM, RS1, RPGR, MERTK, ABCA4, USH2A, MYO7A, CNGA3,* and *CNGB3*-associated retinal disease.[10] ARB should conceivably be amenable to a similar therapeutic approach, and a recent study using gene therapy to treat the canine model of *BEST1*-associated retinopathy confirmed this.[11]

The current study provides a detailed characterisation of the clinical phenotype, genetic findings, and the natural history of ARB in a large number of patients from a single institution, aiming to assist the design of anticipated clinical therapeutic trials for this disease and help inform advice on prognosis.

METHODS

Patient identification and assessment

Clinical records and multimodal retinal imaging of patients with ARB attending a tertiary referral center, Moorfields Eye Hospital in London (UK), were reviewed.[12] Patients known to the eye clinic with a diagnosis of ARB were identified using in-house databases (OpenEyesTM, London). Electronic healthcare records and case notes were then reviewed. All patients included in this database had provided informed consent. This retrospective study adhered to the Tenets of the Declaration of Helsinki and was approved by the Moorfields Eye Hospital ethics committee.

Clinical notes, retinal imaging, and visual electrophysiology were reviewed. Patients' ethnicity was recorded according to the U.S. Department of Health & Human Services (https://ushik.ahrq.gov). Clinical data extracted included visual acuity (VA), refraction, slit-lamp biomicroscopy, and fundoscopy findings. Color fundus photography (CFP), near infrared reflectance imaging (NIR), optical coherence tomography (OCT) scan and fundus autofluorescence (FAF) imaging were reviewed for all patients.

On the basis of the age of onset, we distinguished between patients with adult-onset (> 18 years old) and childhood-onset (< 18 years old) disease.

VA data at first visit (presentation), and at the most recent follow-up (final) visit were analysed. Where necessary, Snellen acuity was converted into logarithm of the minimum angle of resolution (LogMAR). CFP was obtained with either Optos wide-field camera (Optos Panoramic 200; Optos PLC., Scotland, UK) or TRC-50LA Retinal fundus camera (Topcon, Tokyo, Japan). NIR and OCT were performed simultaneously using Spectralis SD-OCT (Heidelberg Engineering, Heidelberg, Germany) for all patients. FAF images were obtained with either a Spectralis HRA OCT (Heidelberg Engineering, Heidelberg, Germany) or Optos widefield camera. When necessary, fluorescein angiography was performed on either the Spectralis or Retinal fundus camera. Visual electrophysiological testing incorporated the International Society of Clinical Electrophysiology of Vision (ISCEV) standards, and included EOG, dark-adapted (DA) and light-adapted (LA) full-field ERG and pattern ERG.[13–15] Change in full-field ERG response over time was assessed by comparing results obtained from patients with ARB to those from unaffected, age-matched control individuals (in-house database, n=140).

Imaging grading

Multimodal imaging including NIR, OCT, FAF and CFP at presentation and most recent follow-up visit were reviewed. OCT analysis included grading for presence of drusen-like vitelliform material (defined as accumulation of subretinal deposits hyperreflective on tomographic scan);[16] outer retinal layer (ORL) thickening (defined as a thicker layer between the RPE and ellipsoid zone interface,[17] corresponding to the interdigitation zone according to the consensus of definitions of OCT nomenclature);[18] the presence of intraretinal fluid (defined qualitatively as > 3 adjacent intraretinal hyporeflective spaces visible on OCT); pigment epithelial detachment (defined as separation between the RPE and Bruch's membrane); and subretinal fluid (SRF). The presence of SRF was further categorised as either diffuse (throughout the whole line scan passing through the fovea) or focal (subfoveal fluid only).

Presence of macular RPE atrophy and macular fibrosis was also assessed. Macular RPE atrophy

153 was defined as single or multiple confluent areas of hyper-reflectivity with sharp margins on NIR, and
154 visible large choroidal vessels on fundus photographs which corresponded to choroidal signal
155 enhancement with loss of RPE and choroidal hypertransmission on the accompanying OCT scans.[19]
156 Macular fibrosis identification was based on fundus photograph, NIR and OCT characteristics. On
157 fundus photographs, fibrosis was said to be present if there were well-delineated areas of yellow-white
158 tissue with corresponding increased reflectivity on NIR and well-defined hyperreflective material on the
159 accompanying OCTs.[19] Central retinal thickness (CRT) from the central 1mm subfield was determined
160 using the Heidelberg software, after manual inspection to ensure correct centration and segmentation.
161 The presence of focal choroidal excavation (FCE)[20] and choroidal neovascularization (CNV)[21,22] were
162 also investigated. CNV was identified on the basis of fluorescein angiography. The nature of material
163 deposited in the subretinal space was also evaluated. Subretinal deposit (SD) was defined as subretinal
164 yellowish material on CFP, with corresponding hyperreflective material on OCT, and increased
165 autofluorescence on FAF, and was classified as either unifocal or multifocal; subfoveal involvement
166 was also assessed. The label of vitelliform material (VM) was reserved for significant collections of
167 coalesced subretinal deposit, such that they resembled the yolk of an egg (Latin = vitellus), as typically
168 observed in patients with autosomal dominant Best disease. All patients were evaluated for the
169 presence of an "inferior track sign" on FAF indicating presumed gravitational tracking of subretinal
170 fluid (chronicity). Where available, Optos widefield images were graded for presence of peripheral
171 drusen-like material, defined as accumulation of subretinal deposits without decreased FAF signal, and
172 presence of RPE atrophy, defined as visible large choroidal vessels with corresponding decreased FAF
173 signal.

174 **Molecular diagnosis**

175 Molecular genetic testing was as part of routine NHS care using single gene Sanger sequencing, or
176 targeted capture next generation sequencing, (National Genetics Reference Laboratory, Manchester
177 Centre for Genomic Medicine, Manchester, UK, and Molecular Vision Laboratory
178 https://www.molecularvisionlab.com/). Some alleles were initially found as part of a whole genome
179 sequencing research projects (NIHR BioResource Rare Diseases Study and the Genomics England

180 study).[23,24] Segregation studies were performed where possible to confirm heterozygous variants were
181 in trans in the affected probands.
182 The nucleotide and peptide variants reported here refer to transcript ENSTxxx and peptide
183 ENSPxxx respectively.

184 **Statistical analysis**

185 Data were analyzed using the Statistical Packages for Social Sciences (SPSS, Version 22, IBM Corp,
186 Armonk, NY). Descriptive statistics were generated for continuous variables and categorical variables.
187 Statistical analysis was mostly descriptive except for the change in VA which was converted from
188 Snellen into LogMAR. Analysis of variance for non-parametric data distribution was used to study the
189 differences in the VA between groups of patients based on the age at the time of diagnosis and on the
190 length of follow-up. For statistical purposes only VA in the right eye was considered for each patient. A
191 cross-sectional analysis was performed for the electrophysiological findings. The chosen level of
192 statistical significance was $p < 0.05$.

193 **RESULTS**

194 56 eyes of 28 unrelated patients were included. Characteristics of patients are summarised in Table 1.
195 At the time of initial examination, the mean age of the cohort was 26.7 ± 15.3 (range 4 - 63) and 10
196 patients were ≤ 18 years old (childhood-onset disease). 13 patients were females. Refractive correction
197 was recorded for 15 patients, with all but one patient being hyperopic (Table 1). Eight patients
198 developed angle closure glaucoma; five of these patients underwent bilateral peripheral laser iridotomy
199 and 4 of these had bilateral clear lens extraction. The most common presenting symptom was reduced
200 central vision (12/18), with a minority of patients presenting with acute angle closure glaucoma (2/28),
201 strabismus (2/18) or as an incidental finding on routine exam (2/18). Presenting symptoms were not
202 available on review of case notes for 10 of 28 patients.

203 **Visual Acuity Progression**

204 Between initial and final assessments, VA declined in the majority of patients (80.4%, mean follow-up
205 8.6 ± 5.3, range 1.7 – 18.8 years). A significant change in VA was detected in patients with ≥ 5 years

follow-up (n = 18) compared to patients with ≤ 5 years follow-up (n = 10, p = 0.001). As a group, the mean presenting VA was 0.52 ± 0.36 LogMAR and final VA was 0.81 ± 0.75 LogMAR (p = 0.06). Younger patients (those ≤ 18 years old) recorded better acuity compared to older patients (p < 0.001). The mean rate of VA decline for children (< 18) was 0.05 ± 0.16 LogMAR/year, the same as for adults, 0.05 ± 0.12 LogMAR/year (p = 1.00). The mean rate of change in VA was 0.05 ± 0.13 LogMAR/year. Right and left eyes did not differ in mean presenting VA (0.55 ± 0.40 LogMAR, p = 0.40), mean final VA (0.74 ± 0.65 LogMAR, p = 0.65), or mean rate of change in VA (0.04 ± 0.10, p = 0.10). Further subgroup analysis was conducted based on presenting VA. This was divided into group 1 (VA </= 0.3 LogMAR), 2 (VA > 0.3 and </= 0.6 LogMAR) and 3 (VA > 0.6 LogMAR). Group 1 had a mean progression 0.15 ± 0.15 LogMAR/year (11 eyes). Group 2 had a mean progression of 0.04 ± 0.04 LogMAR/year (9 eyes, p = 0.30). Group 3 had a mean progression of 0.09 ± 0.17 LogMAR/year (8 eyes, p = 0.78). Figure 2 depicts a scatter plot including the presenting and final BCVA for each patient.

Molecular genetics

Bi-allelic disease-causing variants were identified in each of 27 simplex probands from 27 unrelated families. One patient (case 19) presented with typical clinical, imaging and ERG phenotype of ARB but declined molecular testing (Table 2). Of the 27 patients who did undergo genetic screening, eight were homozygous and 19 were compound heterozygotes for *BEST1* variants.

In total, 31 unique, rare, likely disease-associated variants were reported on the 54 *BEST1* alleles of the 27 probands. These included 18 missense and 13 others predicted to be null alleles (9 protein truncating, 2 mutations affecting a canonical splice donor site sequence, one in-frame deletion of 12 nucleotides (4 amino acids), and one multi-exon deletion).

Bi-allelic missense variants were the most frequently detected combination of pathogenic alleles (12/27), followed by null and missense (9/27), with two null alleles being identified in only a minority of patients (6/27). Pathogenic variants were detected in a homozygous state in 8 patients; two of these cases (patients 5 and 27) with the same ethnicity shared the same variant (c.418C>G, p.(Leu140Val))

without being knowingly related. Compound heterozygous variants were detected in the majority of patients (19/27), with 11 alleles recurring in apparently unrelated individuals, the most common of which is c.422G>A, p.(Arg141His), seen in four unrelated patients 7, 12, 21 and 28. Novel variants were defined as absent from gnomAD (date of access June 18, 2020, v2.1.1) and not previously published or reported in Clinvar. Nine novel variants were identified in our cohort, which included five novel missense and four novel protein truncating variants (Supplemental Table 1).

Comparing the pathogenicity score (CADD PHRED, Supplemental Table 1) of our reported ARB missense variants (n=18) to those reported in gnomAD (n=397) we found it, as expected, to be significantly higher in our ARB variants ($p < 0.001$).

Next we compared the distributions of the peptide coordinates of our ARB missense variants, to those reported to be associated with the dominant form of the disease (ADB) in Clinvar (n=31) and a set of presumed benign missense variants from gnomAD (n = 397). Whilst the distributions of peptide locations for gnomAD was relatively uniform, there was a noticeable difference in the distributions of ARB and ADB peptides with apparent clustering (Supplemental Figure 1). ARB mutations were particularly enriched in the helical domain (amino acid positions 179-199) compared to gnomAD (Supplemental Figure 1).

Imaging findings

Retinal imaging analysis is presented in Table 3. Multimodal retinal imaging of case 1, 12 and 22 are represented in Figures 1, 3, 4 and 5. There was evidence of a high degree of inter-ocular symmetry. The most prevalent imaging finding at presentation was subretinal deposit (SD), which was found in the majority of eyes (80.3%, 45/56); and most frequently multifocal (69.6%, 39/56), with macular involvement in 17.85% of eyes (10/56). Prevalence of SD did not increase over time. At final follow-up, a single vitelliform lesion, as is typically observed in patients with autosomal dominant Best disease, was present in two patients with ARB. Tomographic evidence of ORL thickening was identified in 46.4% of eyes (13/28), at both the initial and final examination.

SRF was found in the majority of eyes (75%, 42/56) at presentation; the location of SRF was

258 subfoveal in almost one-half of these eyes, and diffuse (involving the whole OCT line scan) in the
259 remaining patients. The presence of SRF did not change significantly over time, since it was found in
260 the same proportion of eyes (75%, 42/56) at the last visit. More than one-half of the eyes (57%, 32/56)
261 presented with IRF, which remained relatively stable over time.

262 At presentation, macular RPE atrophy was identified in 39.2% of eyes (11/28), whereas macular
263 fibrosis was found in a relatively small proportion of eyes (25%, 7/28). RPE atrophy and macular
264 fibrosis were found in slightly more eyes at the last follow-up visit (Table 3).

265 Between initial and final OCT examinations, the majority of patients (80.4%) recorded a
266 reduction in central retinal thickness (CRT) in the central 1 mm subfield. Mean CRT at baseline was
267 362μm ± 139μm (range 147μm – 754μm), and at final follow-up was 349μm ± 168μm (range 134μm –
268 895μm, p-value = 0.58). Subjectively, variation in CRT appeared to correlate with the degree of IRF,
269 rather than outer retinal atrophy. In this cohort of patients. Mean initial CRT in younger patients (≤18
270 years old) was 403μm ± 75μm, whilst in adult patients it was 339μm ± 160μm (p = 0.10). The majority
271 of patients in both age-groups (≤ 18 years old, 90%; > 18 years, 75%) had a documented reduction in
272 CRT at final follow-up.

273 During the initial examination, FCE was detected in four eyes of three patients, and at the last
274 follow-up visit in eight eyes of five patients (Figure 3). In these eyes FCE was not associated with
275 evidence of Type 1 macular neovascular disease, however in 5/8 eyes flat, irregular pigment epithelial
276 detachments (PED) were present, associated with subretinal hyperreflective material (SHRM) in three
277 cases, hinting that FCE may be associated with a relatively indolent Type 2 neovascular lesion. One eye
278 of one patient developed a Type 1 neovascular lesion without FCE (previously published), which did
279 not require treatment.[17,18]

280 Changes in short wavelength fundus autofluorescence were identified in all patients –
281 hyperautofluorescence was observed in regions with ORL thickening, subretinal deposit and subretinal
282 fluid, and hyperautofluorescence in regions of outer retinal atrophy. Gravitational tracks were noted in
283 six eyes of six patients at the initial visit and in eleven eyes of six patients at the final visit (Figure 4).

Qualitative longitudinal analysis identified an enlargement in the area of macular hypoautofluorescence in 14.3% of patients. For almost all patients, changes in fundus autofluorescence spared the peripapillary retina (26 of 28, 92.9%).

Ultra-widefield imaging (Optos) was obtained in 42 eyes of 21 patients. Peripheral drusen-like material was visible in 19 eyes of 10 patients. Ten eyes of six patients manifested patches of peripheral RPE atrophy. All patients with peripheral atrophy had evidence of peripheral (presumed subretinal) drusen-like material (Figure 5).

Electrophysiological findings

Electroretinography data were available for 26 patients, and EOG data for 24 patients. In all cases a severe reduction in the EOG light peak to dark trough (LP:DT) ratio was detected, disproportionate to the ERG reduction in the majority and in keeping with severe generalised dysfunction of the RPE. Severe EOG abnormality occurred in patients of all ages, and showed a high degree of inter-ocular symmetry (Figure 6A; median LP:DT ratio 100%; maximum 125%; age range 9-63 years).

Pattern ERGs were available in 51 eyes of 26 cases. PERG P50 was abnormal in 43 eyes, consistent with macular dysfunction, including 24 eyes from 13 subjects with undetectable responses. There was marked (> 50%) inter-ocular amplitude asymmetry in 4 subjects (Figure 6B and 6C). Pattern ERGs were normal in 9 of 10 eyes including both eyes from four children aged 9-13 years (Figure 6C). Full-field ERGs were available in 26 cases and the main components and inter-ocular symmetry summarised in Figure 7. The dark adapted (DA) 0.01 (dim flash) and DA 10 (strong flash) ERG mean a- and b-wave amplitudes were 34%, 42% and 30% smaller respectively than in the control group; light adapted (LA) 30Hz (flicker) and LA 3 (single flash cone) ERG mean amplitudes were 32% and 25% smaller respectively than in the control group. The mean peak time difference between patients and controls was 6ms for the DA10 ERG b-wave and 5ms for the LA 30Hz ERG.

The DA and LA ERGs indicated greater rod than cone involvement (n = 10 cases), similar severity of rod and cone system dysfunction (n = 5), isolated rod dysfunction (n = 4), cone more than rod dysfunction (n = 1) or mild cone system involvement only (n = 2). Four patients had normal full-

field ERGs. Patients with normal full-field ERGs were significantly younger than those with abnormal ERGs (10.7 ± 3.9 years versus 33.5 ± 16.8 years, p = 0.0004), and had better VA (0.18 ± 0.13 LogMAR versus 0.57 ± 0.48 LogMAR, p = 0.02).

The main DA and LA ERG components showed reduction and increased peak times that tended to be worse in older cases; the mean rate of amplitude decline was similar or slightly worse than in the unaffected control group (Supplemental Figure 2).

Two subjects (aged 12 and 27 years at baseline) were monitored over periods of 12 years and 5 years respectively. Both had undetectable pattern ERGs. In the younger subject DA10 ERG a and b-waves declined by 60% and 30% respectively; LA 30Hz ERGs declined by 42% and increased in peak time by 8ms (Figure 8A). In the older subject DA 10 ERG a- and b-waves declined by 30% and 25%; LA 30Hz ERGs by 12% and peak time increased by 7ms (Figure 8B). The rate of DA ERG reduction was greater and rate of LA ERG reduction similar to that suggested by the age-dependency suggested by the cross-sectional analysis.

DISCUSSION

Since the recent approval of voretigene neparvovec-rzyl (Luxturna) for biallelic *RPE65*-associated retinal dystrophy, there has been a growing interest in gene therapy for monogenic inherited retinal dystrophies (IRDs). ARB results from biallelic variants in *BEST1* and is considered the null phenotype. As such, ARB represents a possible candidate for gene replacement therapy, an idea that was recently strengthened by the promising results of *BEST1* gene supplementation in the canine model of ARB.[11]

The present work systematically reviews the clinical and molecular features associated with ARB, representing, to the best of our knowledge, the largest series of patients to date. Unlike other early-onset retinal dystrophies, children with ARB typically develop good central vision, evidenced by the near normal acuity and robust PERG responses observed in the first decade of life. The risk of amblyopia is therefore low, as long as any associated refractive error and strabismus are corrected. Subsequently, often commencing in the teenage years, macular function declines, although this is highly variable. Whilst the overall trend was towards a decrease in VA over the duration of follow-up (p =

336 0.06), for the group as a whole, this did not reach statistical significance. In subgroup analyses however,
337 poorer VA outcomes were identified in older patients (> 18 versus ≤ 18 years old, $p < 0.001$), and
338 those with longer follow-up (≥ 5 years versus < 5 years, $p = 0.001$), supporting the concept of
339 progressive deterioration. Overall, the mean rate of progression was 0.05 ± 0.11 LogMAR / year,
340 which is very similar to that observed in a recent cross-sectional cohort study of Stargardt Disease (0.05
341 LogMAR/year).[25] A decline in visual function is also suggested by the higher prevalence of full-field
342 ERG abnormalities in older compared to younger patients. Typically, these affect the rod system more
343 than cone pathways. Where serial ERGs were performed on the same patient (n = 2), decline greater
344 than that expected for age was evident. While this gradual deterioration provides a wide potential
345 therapeutic window, this is a childhood onset disorder and the progression may be difficult to predict.
346 Intervention is likely to be most effective if delivered early in the disease course, and certainly prior to
347 vision limiting complications such as macular atrophy and fibrosis.

348 We were also able to identify changes in retinal structure over time, with the majority of
349 patients (80.4%) recording a reduction in retinal thickness during follow-up (mean follow-up 8.6 years).
350 Whilst CRT is influenced by other factors, such as the degree of intra or sub-retinal fluid, the high
351 proportion of patients recording a reduction in CRT supports the notion of progressive outer retinal
352 atrophy. Loss of outer retinal structure may be expected to alter macular autofluorescence
353 characteristics; here this was observed in 14% of patients. Macular neovascularisation and FCE were
354 two further independent structural changes that were identified that could potentially influence final
355 visual prognosis. Flat irregular PEDs were often observed in association with FCEs, sometimes with
356 overlying SHRM; one may speculate that a neovascular lesion growing in the sub-RPE space may
357 compromise superficial choroidal anatomy, and cause FCE, more readily than a neovascular membrane
358 that expands into the sub-retinal space. In addition, sub-RPE (Type 1) neovascular lesions are less likely
359 to result in dramatic, acute haemorrhagic or exudative consequences, and so be overlooked. It is
360 interesting to note that of all monogenic retinal dystrophies, the highest prevalence of FCE is seen in
361 association with variants in *BEST1*. In addition to the retinopathy, it is also important to remember

362 that abnormal iridocorneal anatomy, shallow anterior chamber depth and reduced axial length all
363 predispose to an increased prevalence of angle closure glaucoma in patients with ARB, another factor
364 which may complicate both the delivery and response to novel therapies delivered into the vitreous or
365 subretinal space.

366 Many of the imaging findings in ARB have been previously associated with Best disease,
367 however fundoscopy, retinal imaging, and electrophysiology findings usually distinguish these two
368 disorders.[26] An intermediate group of patients do exist who harbour heterozygous pathogenic *BEST1*
369 variant associated with mild, but multifocal subretinal deposit (multifocal Best disease).[27] It remains to
370 be determined if these patients truly have autosomal dominant disease, or, if in fact they harbour an
371 undetected second disease causing allele, and thus represent a milder presentation of ARB. Similarly,
372 when bi-allelic variants in *BEST1* are identified, there appears to be a spectrum of retinal dysfunction,
373 with a variable age of onset of symptoms. The median age of carriers of a null allele (n = 15) was lower,
374 19 years old, than in non-carriers (n = 12), 29 years old, although the difference was not statistically
375 significant. Further, the median VA in the right eye at presentation was lower at 0.4 LogMAR in null
376 allele carriers than in non-carriers, 0.6 LogMAR, but not significant. It is likely that rather than ARB
377 representing the null phenotype, patients with these constellation of signs have significantly reduced
378 BEST1 function, and this may vary between no functional protein in those who are nullizygous, and
379 partial function, in those with at least one hypomorphic, usually missense, variants associated with a
380 milder disease with a later-onset. Whilst null alleles may be expected to occur throughout the gene,
381 dominantly acting variants conferring a gain of function should occur at specific residues with
382 functional importance, as observed in autosomal dominant Best disease. Similarly hypomorphic
383 recessive missense variants that partially reduce BEST1 function would be expected to cluster around
384 in key domains; both hypotheses are supported by our data (Supplemental Figure 1). A recent report by
385 Shah et al. describing a cohort of patients with *BEST1* sequence variations included 18 patients from nine
386 families with ARB.[28] Missense variants were identified in all probands , in contrast to the present series, where
387 null alleles were discovered in 42% of cases. The most commonly identified variant in both cohorts was
388 p.(Arg141His),

In anticipation of therapeutic trials, robust biomarkers associated with ARB disease activity are sought. Unlike many rod-cone or cone-rod dystrophies, there is no clear evidence of centrifugal or centripetal progression in patients with ARB, complicating the process of characterising change in retinal structure. The present work suggests that conventional endpoints such as ETDRS letter score, and OCT derived measurements of retinal thickness are likely to be helpful, and although there are suggestions that electroretinography and fundus autofluorescence imaging may quantify changes in the long term (> 5 years), their utility in the short-term (< 5 years) remains to be determined. Other techniques used to assess change in visual function, such as change in electro-oculography and static perimetry, or retinal structure, such as volume of vitelliform material/fluid in the subretinal space, to date remain poorly studied in patients with ARB.

Our findings are consistent with those of other bestrophinopathies in which there is progressive visual worsening over time with a rate of decline which is typically slow, providing a long therapeutic window, as central photoreceptors remain viable for decades despite the persistence of SRF.[29] These observations are also in line with another report,[26] and support the idea that the retina may be preserved in childhood and that early treatment with gene replacement therapy may be effective in preventing later photoreceptor cell death. To date, most clinical trials of novel therapies for IRD have taken advantage of the symmetrical findings expected in these conditions. Whilst most potential outcome measures were found to be highly concordant between eyes (e.g. best corrected visual acuity, central retinal thickness), in a minority of subjects (4/26) the PERGs revealed a marked inter-ocular difference, in spite of otherwise symmetrical electrophysiology, and likely to be an important consideration when considering potential treatment strategies – including potentially posing challenge in using the fellow untreated eye as a control. Of all IRDs, variants in *BEST1* appear to be most associated with unilateral or asymmetric disease.[30] An additional factor to consider when delivering novel therapies to the macula is the association between ARB and sub/intraretinal fluid. Here, SRF was found in the vast majority of eyes, and IRF in more than one-half of the eyes. Whilst subretinal delivery of gene-replacement therapy may be less traumatic in the presence of SRF, it is likely to be more challenging if associated with IRF

due to the likely greater risk of macular hole formation.[31] Spontaneous fluctuations in IRF are also likely to impact on visual function, independently of any response to treatment, complicating the interpretation of visual outcome measures.

Limitations of this study that could be addressed in future work include its retrospective and predominantly cross-sectional nature, and lack of standardised protocols applied to all patients. A multi-centred approach is likely to be required to significantly increase the number of patients studied, and in preparation for clinical trials this may be possible.

In conclusion, the detailed clinical, imaging, electrophysiological and genetic findings of our large case series of patients with ARB will help to better inform discussions with patients regarding their prognosis, facilitate genetic counselling, and moreover, add to the published data to help optimise the clinical design of anticipated interventional studies, as well as providing a pool of well-characterised potential participants.

427 **REFERENCES**

428 1. Boon CJF, Klevering BJ, Leroy BP, Hoyng CB, Keunen JEE, den Hollander AI. The spectrum
429 of ocular phenotypes caused by mutations in the BEST1 gene. *Prog Retin Eye Res*. 2009;28(3):187-
430 205. doi:10.1016/j.preteyeres.2009.04.002

431 2. Johnson AA, Guziewicz KE, Lee CJ, et al. Bestrophin 1 and retinal disease. *Prog Retin Eye Res*.
432 2017;58:45-69. doi:10.1016/j.preteyeres.2017.01.006

433 3. Marmorstein AD, Marmorstein LY, Rayborn M, Wang X, Hollyfield JG, Petrukhin K.
434 Bestrophin, the product of the Best vitelliform macular dystrophy gene (VMD2), localizes to the
435 basolateral plasma membrane of the retinal pigment epithelium. *Proc Natl Acad Sci U S A*.
436 2000;97(23):12758-12763. doi:10.1073/pnas.220402097

437 4. Sun H, Tsunenari T, Yau KW, Nathans J. The vitelliform macular dystrophy protein defines a
438 new family of chloride channels. *Proc Natl Acad Sci U S A*. 2002;99(6):4008-4013.
439 doi:10.1073/pnas.052692999

440 5. Dickson VK, Pedi L, Long SB. Structure and insights into the function of a Ca2+-activated Cl-
441 channel. *Nature*. 2014;516(7530):213-218. doi:10.1038/nature13913.Structure

442 6. Yang T, Liu Q, Kloss B, et al. Structure and Selectivity in Bestrophin Ion Channels Tingting.
443 *Science (80-)*. 2014;346(6207):355-359. doi:10.1126/science.1259723.Structure

444 7. Rahman N, Georgiou M, Khan KN, Michaelides M. Macular dystrophies: Clinical and imaging
445 features, molecular genetics and therapeutic options. *Br J Ophthalmol*. 2020;104(4):451-460.
446 doi:10.1136/bjophthalmol-2019-315086

447 8. Schatz P, Klar J, Andréasson S, Ponjavic V, Dahl N. Variant phenotype of Best vitelliform
448 macular dystrophy associated with compound heterozygous mutations in VMD2. *Ophthalmic*
449 *Genet*. 2006;27(2):51-56. doi:10.1080/13816810600677990

450 9. Burgess R, Millar ID, Leroy BP, et al. Biallelic Mutation of BEST1 Causes a Distinct
451 Retinopathy in Humans. *Am J Hum Genet*. 2008;82(1):19-31. doi:10.1016/j.ajhg.2007.08.004

452 10. Lee JH, Wang JH, Chen J, et al. Gene therapy for visual loss: Opportunities and concerns. *Prog*

453 *Retin Eye Res*. 2019;68(August 2018):31-53. doi:10.1016/j.preteyeres.2018.08.003

454 11. Guziewicz KE, Cideciyan A V., Beltran WA, et al. BEST1 gene therapy corrects a diffuse retina-
455 wide microdetachment modulated by light exposure. *Proc Natl Acad Sci U S A*.
456 2018;115(12):E2839-E2848. doi:10.1073/pnas.1720662115

457 12. Pontikos N, Arno G, Jurkute N, et al. Genetic Basis of Inherited Retinal Disease in a
458 Molecularly Characterized Cohort of More Than 3000 Families from the United Kingdom.
459 *Ophthalmology*. 2020:1-11. doi:10.1016/j.ophtha.2020.04.008

460 13. McCulloch DL, Marmor MF, Brigell MG, et al. ISCEV Standard for full-field clinical
461 electroretinography (2015 update). *Doc Ophthalmol*. 2015;130(1):1-12. doi:10.1007/s10633-014-
462 9473-7

463 14. Bach M, Brigell MG, Hawlina M, et al. ISCEV standard for clinical pattern electroretinography
464 (PERG): 2012 update. *Doc Ophthalmol*. 2013;126(1):1-7. doi:10.1007/s10633-012-9353-y

465 15. Constable PA, Bach M, Frishman LJ, Jeffrey BG, Robson AG. ISCEV Standard for clinical
466 electro-oculography (2017 update). *Doc Ophthalmol*. 2017;134(1):1-9. doi:10.1007/s10633-017-
467 9573-2

468 16. Khan KN, Mahroo OA, Khan RS, et al. Differentiating drusen: Drusen and drusen-like
469 appearances associated with ageing, age-related macular degeneration, inherited eye disease and
470 other pathological processes. *Prog Retin Eye Res*. 2016;53:70-106.
471 doi:10.1016/j.preteyeres.2016.04.008

472 17. Querques G, Regenbogen M, Quijano C, Delphin N, Soubrane G, Souied EH. High-Definition
473 Optical Coherence Tomography Features in Vitelliform Macular Dystrophy. *Am J Ophthalmol*.
474 2008;146(4):501-508. doi:10.1016/j.ajo.2008.05.029

475 18. Staurenghi G, Sadda S, Chakravarthy U, Spaide RF. Proposed lexicon for anatomic landmarks in
476 normal posterior segment spectral-domain optical coherence tomography: The IN•OCT
477 consensus. *Ophthalmology*. 2014;121(8):1572-1578. doi:10.1016/j.ophtha.2014.02.023

478 19. Casalino G, Stevenson MR, Bandello F, Chakravarthy U. Tomographic Biomarkers Predicting

479 Progression to Fibrosis in Treated Neovascular Age-Related Macular Degeneration: A
480 Multimodal Imaging Study. *Ophthalmol Retin*. 2018;2(5):451-461. doi:10.1016/j.oret.2017.08.019
481 20. Parodi MB, Casalino G, Iacono P, Introini U, Adamyan T, Bandello F. The expanding clinical
482 spectrum of choroidal excavation in macular dystrophies. *Retina*. 2018;38(10):2030-2034.
483 doi:10.1097/IAE.0000000000001805
484 21. Khan KN, Mahroo OA, Islam F, Webster AR, Moore AT, Michaelides M. Functional and
485 Anatomical Outcome of Choroidal Neovascularization Complication BEST1-Related
486 Retinopathy. *Retina*. 2017;37(7):1360-1370. doi:10.1097/IAE.0000000000001357
487 22. Introini U, Casalino G, Khan KN, et al. Clinical course of autosomal recessive bestrophinopathy
488 complicated by choroidal neovascularization. *Ophthalmic Surg Lasers Imaging Retin*.
489 2018;49(11):888-892. doi:10.3928/23258160-20181101-10
490 23. Carss K, Arno G, Erwood M, et al. Comprehensive Rare Variant Analysis via Whole-Genome
491 Sequencing to Determine the Molecular Pathology of Inherited Retinal Disease. *Am J Hum*
492 *Genet*. 2017;100(1):75-90. doi:10.1016/j.ajhg.2016.12.003
493 24. Ouwehand WH. Whole-genome sequencing of rare disease patients in a national healthcare
494 system. *BioRxiv*. 2020. doi:10.1101/507244
495 25. Strauss RW, Muñoz B, Ahmed MI, et al. The Progression of the Stargardt Disease Type 4
496 (ProgStar-4) Study: Design and Baseline Characteristics (ProgStar-4 Report No. 1). *Ophthalmic*
497 *Res*. 2018;60(3):185-194. doi:10.1159/000491791
498 26. Borman AD, Davidson AE, O'Sullivan J, et al. Childhood-Onset Autosomal Recessive
499 Bestrophinopathy. *Arch Ophtahlmol*. 2011;129(8):1088-1093.
500 doi:10.1017/CBO9781107415324.004
501 27. Boon CJF, Klevering J, Den Hollander AI, et al. Clinical and genetic heterogeneity in multifocal
502 vitelliform dystrophy. *Arch Ophthalmol*. 2007;125(8):1100-1106. doi:10.1001/archopht.125.8.1100
503 28. Shah M, Broadgate S, Shanks M, et al. Association of Clinical and Genetic Heterogeneity with
504 BEST1 Sequence Variations. *JAMA Ophthalmol*. 2020;138(5):544-551.

505 doi:10.1001/jamaophthalmol.2020.0666

506 29. Yang T, Justus S, Li Y, Tsang SH. BEST1: The Best Target for Gene and Cell Therapies. *Mol*
507 *Ther*. 2015;23(12):1805-1809. doi:10.1038/mt.2015.177

508 30. Arora R, Khan K, Kasilian ML, et al. Unilateral BEST1-Associated Retinopathy. *Am J*
509 *Ophthalmol*. 2016;169:24-32. doi:10.1016/j.ajo.2016.05.024

510 31. Xue K, Groppe M, Salvetti AP, MacLaren RE. Technique of retinal gene therapy: Delivery of
511 viral vector into the subretinal space. *Eye*. 2017;31(9):1308-1316. doi:10.1038/eye.2017.158

512

513 **FIGURE LEGENDS**

514 **Figure 1.** Multimodal retinal imaging of case 22 (p.Tyr97Ter and p.Leu41Pro mutations in *BEST1*). **A**
515 **and B,** Wide field color image shows multifocal vitelliform material (VM) in both eyes. **C and D,** Wide
516 field fundus autofluorescence (AF) and **E and F,** fundus autofluorescence (55° degrees) show marked
517 increased AF in correspondence of the VMs (black asterisks). **G**, Spectral-domain optical coherence
518 tomography (SD-OCT) scan of both eyes show subretinal drusen-like deposits (white asterisks),
519 subretinal fluid, outer retinal layer thickening, and intraretinal fluid.

520 **Figure 2.** Scatter plot depicting best-corrected visual acuity (LogMAR) as a function of age (years).
521 Vision for the right eye at baseline (on first presentation to our facility) and at final follow-up is
522 depicted for each patient as per the legend.

523 **Figure 3.** Spectral-domain optical coherence tomography (SD-OCT) scan of case 12 at presentation (**A**
524 **and B**) and at last follow-up visit (**C and D**). **A and B,** SD-OCT scan at presentation shows well
525 defined subretinal hyperreflectivity consistent with vitellifom material (yellow asterisks), subretinal fluid,
526 outer retinal layer thickening (red arrows) and elongation of the photoreceptor outer segments
527 ("stalactites"). **C,** SD-OCT scan of the right eye show persistent subretinal fluid, a focal choroidal
528 excavation (yellow arrow) and back scattering of the signal in the choroid consistent with retinal
529 pigment epithelium (RPE) atrophy (yellow asterisks). **D,** SD-OCT scan of the left eye show persistence
530 of subretinal fluid and RPE atrophy at the macula (yellow asterisks).

531 **Figure 4.** Optos widefield imaging of case 12 (p.Arg141His and p.Gln159Ter mutations in BEST1). **A**
532 **and B,** Wide field color image shows unifocal subfoveal vitelliform material in both eyes (white
533 asterisks). **C and D,** Wide field fundus autofluorescence (AF) shows marked increased AF at the
534 posterior pole and increased AF ("gravitational tract") tracking inferior to the macula (yellow arrows).

535 **Figure 5.** Multimodal retinal imaging of case 1 (BEST1:p.Gly34Gly; p.Leu191Pro compound
536 heterozygous). **A and B,** Wide field color image shows peripheral drusen-like material (white
537 arrowheads) and patches of RPE atrophy in the periphery of both eyes (white arrows). **C and D,** Wide
538 field fundus autofluorescence (AF) shows marked AF changes at the posterior pole and in the mid

539 periphery and decreased AF signal in correspondence of patches of RPE atrophy (white arrows). **E**
540 **and F,** Fundus autofluorescence (55° degrees). **G,** Spectral-domain optical coherence tomography (SD-
541 OCT) scan of the right eye shows cystoid macular degeneration (white arrow) and subretinal drusen-
542 like deposits (yellow arrowhead). **H,** SD-OCT scan of the left eye shows a shallow pigment epithelial
543 detachment (yellow asterisk).

544 **Figure 6. A,** The EOG light peak to dark trough ratio was grossly abnormal bilaterally (median 100%)
545 irrespective of age. The broken line shows the lower limit of normal. **B,** Pattern ERG P50 amplitude in
546 right (RE) and left (LE) eyes. The P50 component was subnormal in the majority and undetectable
547 bilaterally in 11 cases (large filled circle). Four showed an inter-ocular asymmetry greater than 50%. The
548 broken line shows the lower limit of normality. **C,** Pattern ERGs were normal in 9 of 10 eyes including
549 both eyes from 4 children aged 9-13 years

550 **Figure 7.** The main ERG component amplitudes and peak times recorded from right (RE) and left
551 (LE) eyes. Amplitudes are compared for the DA0.01 ERG (**A**), DA 10 ERG a-wave (**B**) and b-wave
552 (**C**) and LA 30Hz ERGs (**E**). Peak times are compared for the DA 10 ERG b-wave (**D**) and LA 30Hz
553 flicker ERG (**F**).

554 **Figure 8.** Comparison of the main ERG component amplitudes obtained at baseline and follow up in
555 a 12-year-old (**A**) and 27-year-old (**B**) subject, monitored over 12 years and 5 years respectively. The
556 LA 30Hz peak time in the younger subject increased by 8ms after 12 years and by 7ms in the older case
557 after 5 years.

558 **Supplemental Figure 1.** Spatial clustering of missense mutations in BEST1. **A,** Histograms of the
559 amino acid positions of missense variants in our ARB patients, (n=18), in ADB patients from Clinvar
560 (n=31) and in controls from gnomAD (n=397) relative to ATG start codon (Met = 1). **B,** Tertiary
561 structure of BEST1 region highlighting clustering of ARB missense variants (green) and ADB missense
562 variants (red). **C,** Secondary structure of BEST1 with ARB missense variants (green) and ADB
563 missense variants (red).

564 **Supplemental Figure 2.** The main ERG amplitude and peak times as a function of age, compared
565 with those for an unaffected control group. Amplitude and peak time data are shown for the DA 0.01
566 ERG (**A, B**), the DA10 ERG a-wave (**C**, **D**) and b-wave (**E**, **F**), LA 30Hz ERG (**G, H**) and LA 3 ERG
567 b-wave (**I**, **J**). The largest amplitude response shown in **A**, **C**, **E**, **G** and **I** (all recorded from the same
568 young subject) are excluded from the linear regression (solid line). Linear regression for the control
569 group is shown for comparison (broken line).

570 **Supplemental Table 1.** Summary of *BEST1* variants found in our cohort. The variants found are
571 specified; as are the patients with these variants, whether the mutation is novel (reported here first), the
572 predicted effect on the protein, the variant class, the human genome build variant ID, Gnomad allele
573 frequency, Pubmed ID, ACMG classification and CADD pathogenicity score. Abbreviations: ACMG:
574 American College of Medical Genetics guidelines; b37_variant_ID – human genome build 37;
575 b38_variant _id – human genome build 38; CADD – Combined Annotation Dependent Depletion
576 score; HGVSs – Human Genome Variation Society cDNA nomenclature; PTV – protein truncating
577 variant.

No	Gender	Race	Age (years)	Refraction		VA (LogMAR) First visit		VA (LogMAR) Last visit		PACG	Follow-up (years)
				OD	OS	OD	OS	OD	OS		
1	F	White	34	Unknown	Unknown	0.30	0.78	3.00	0.82	yes	17
2	M	White	39	+4.00	+4/-0.50@70	1.00	1.00	1.00	1.00	yes	14
3	M	Asian	49	+2/-0.50@120	+2/-0.75@70	0.78	0.78	0.78	0.78	no	15
4	M	White	30	Unknown	Unknown	0.60	0.60	0.60	0.60	no	11
5	M	Asian	22	Unknown	Unknown	1.00	1.00	1.00	1.00	no	12
6	F	White	44	+2.50	+4.00	0.60	0.48	0.90	0.90	no	15
7	F	White	27	+4.00	+4.00	0.78	1.00	0.60	1.30	no	18
8	M	White	48	Unknown	Unknown	0.48	0.48	1..60	1.60	no	14
9	M	White	36	Unknown	Unknown	0.48	1.00	0.48	0.78	no	7
10	F	Asian	35	Unknown	Unknown	1.00	0.78	1.60	1.60	yes	12
11	F	Unknown	16	+1.25/+1@75	+1.00	0.18	0.48	0.18	0.48	yes	12
12	F	White	5	+6/-1@180	+5/-0.75@50	0.10	0.10	0.90	0.20	no	11
13	M	African	19	Unknown	Unknown	0.48	0.30	1.00	0.8	no	10
14	M	White	4	+4.50	+3.50	0.10	0.10	0.10	0.00	no	11
15	M	White	14	Unknown	Unknown	0.40	0.78	1.00	1.00	no	9
16	M	Unknown	11	+6/-0.75@110	+5.25/-1@80	0.32	0.02	0.18	0.00	no	8
17	M	Asian	40	Unknown	Unknown	0.60	0.30	0.60	0.60	yes	9
18	M	Unknown	12	-0.50	-0.25	0.06	0.40	0.00	0.00	no	8
19	F	White	15	+4.00	+3.00	0.56	0.10	0.42	0.02	no	2
20	M	White	45	Unknown	Unknown	1.60	1.60	3.00	3.00	no	3
21	F	White	25	Unknown	Unknown	0.78	1.18	1.00	1.60	yes	4
22	F	White	12	+0.50	+0.75/-0.25@5	0.30	0.28	0.48	0.48	no	4
23	M	African	12	+1.00	+0.25	0.30	0.28	0.18	0.30	no	3
24	M	African	31	-1.00	-1.25	0.18	0.18	0.30	0.18	no	1
25	F	White	63	Unknown	Unknown	0.30	0.78	0.30	0.60	no	3
26	F	White	31	+2.50	+3.00	0.30	0.18	0.18	0.18	yes	2
27	F	Asian	7	+5/-1@180	+6/-2@180	0.12	0.20	0.40	0.50	no	1
28	F	White	22	Unknown	Unknown	0.78	0.30	1.00	0.48	yes	2

Table 1. Demographic characteristics, refraction, visual acuity, presence of glaucoma and years of follow-up of patients included. The abbreviations are as follows: PACG = primary angle-closure glaucoma; VA = visual acuity.

No	Variant 1	Predicted effect	Variant 2	Predicted effect
1	c.102C>T	p.Gly34Gly	c.572T>C	p.Leu191Pro
2	c.102C>T	p.Gly34Gly	c.1470_1471delCA	p.His490GlnfsTer24
3	c.-29+1G>T	splicing	c.-29+1G>T	splicing
4	*c.1014G>A*	p.Trp338Ter	c.-29+1G>T	splicing
5	c.418C>G	p.Leu140Val	c.418C>G	p.Leu140Val
6	c.454C>G	p.Pro152Ala	c.122T>C	p.Leu41Pro
7	c.122T>C	p.Leu41Pro	c.422G>A	p.Arg141His
8	c.454C>G	p.Pro152Ala	c.584C>T	p.Ala195Val
9	c.598C>T	p.Arg200Ter	c.598C>T	p.Arg200Ter
10	c.107_118delAGTACGAGAACC	p.Gln36_Asn39del	c.107_118delAGTACGAGAACC	p.Gln36_Asn39del
11	c.1038dupC	p.Tyr347LeufsTer54	*c.533A>C*	p.His178Pro
12	c.422G>A	p.Arg141His	c.475C>T	p.Gln159Ter
13	c.636+1G>C	splicing	c.636+1G>C	splicing
14	c.584C>T	p.Ala195Val	c.974T>C	p.Met325Thr
15	c.1066C>T	p.Arg356Ter	exon 1 to 2 deletion	N/A
16	c.1066C>T	p.Arg356Ter	c.550C>T	p.Pro184Ser
17	c.468C>G	p.His156Gln	c.468C>G	p.His156Gln
18	c.1066C>T	p.Arg356Ter	c.602T>C	p.Ile201Thr
19	declined genetic testing			
20	c.974T>C	p.Met325Thr	c.602T>C	p.Ile201Thr
21	c.29C>T	p.Ala10Val	c.422G>A	p.Arg141His
22	c.291C>G	p.Tyr97Ter	c.122T>C	p.Leu41Pro
23	c.74G>A	p.Arg25Gln	c.278G>A	p.Trp93Ter
24	c.530C>T	p.Pro177Leu	c.169G>T	p.Glu57Ter
25	c.1038dupC	p.Tyr347LeufsTer54	c.421C>A	p.Arg141Ser
26	c.728C>A	p.Ala243Glu	c.728C>A	p.Ala243Glu
27	c.418C>G	p.Leu140Val	c.418C>G	p.Leu140Val
28	c.422G>A	p.Arg141His	c.839A>C	p.Gln280Pro

Table 2. List of detected variants in the subjects enrolled.

SPECTRALIS OCT AND FAF EXAMINATION			
		Presentation	**Last Follow-up**
Macular SD			
	Subfoveal	12 (6)	10 (5)
	Unifocal	6 (3)	4 (2)
	Multifocal	39 (20)	39 (20)
SRF			
	Any	42 (22)	42 (22)
	Subfoveal	20 (12)	20 (11)
	Diffuse	22 (10)	22 (11)
IRF		32 (16)	34 (17)
ORL Thickening		25 (13)	24 (12)
PED		3 (2)	4 (4)
FCE		3 (2)	8 (5)
Gravitational Track		6 (6)	11 (6)
Macular RPE Atrophy		11 (6)	13 (7)

OPTOS COLOUR AND FAF EXAMINATION	
Peripheral Drusen-Like Material	19 (10)
Peripheral Atrophy	10 (6)

Table 3. Retinal imaging findings at presentation and at last follow-up visit. Findings are seperated by imaging platform as specified. Spectralis imaging was available for 56 patients and Optos imaging from 21 patients. The number of affected eyes is specified with the number of patients in parenthesis. The abbreviations are as follows: CMD = cystoid macular degeneration; FCE = focal choroidal excavation; IRF = intraretinal fluid; ORL = outer retina layers; PED = pigment epithelial detachment; RPE = retinal pigment epithelium; SD = subretinal deposit; SRF = subretinal fluid.

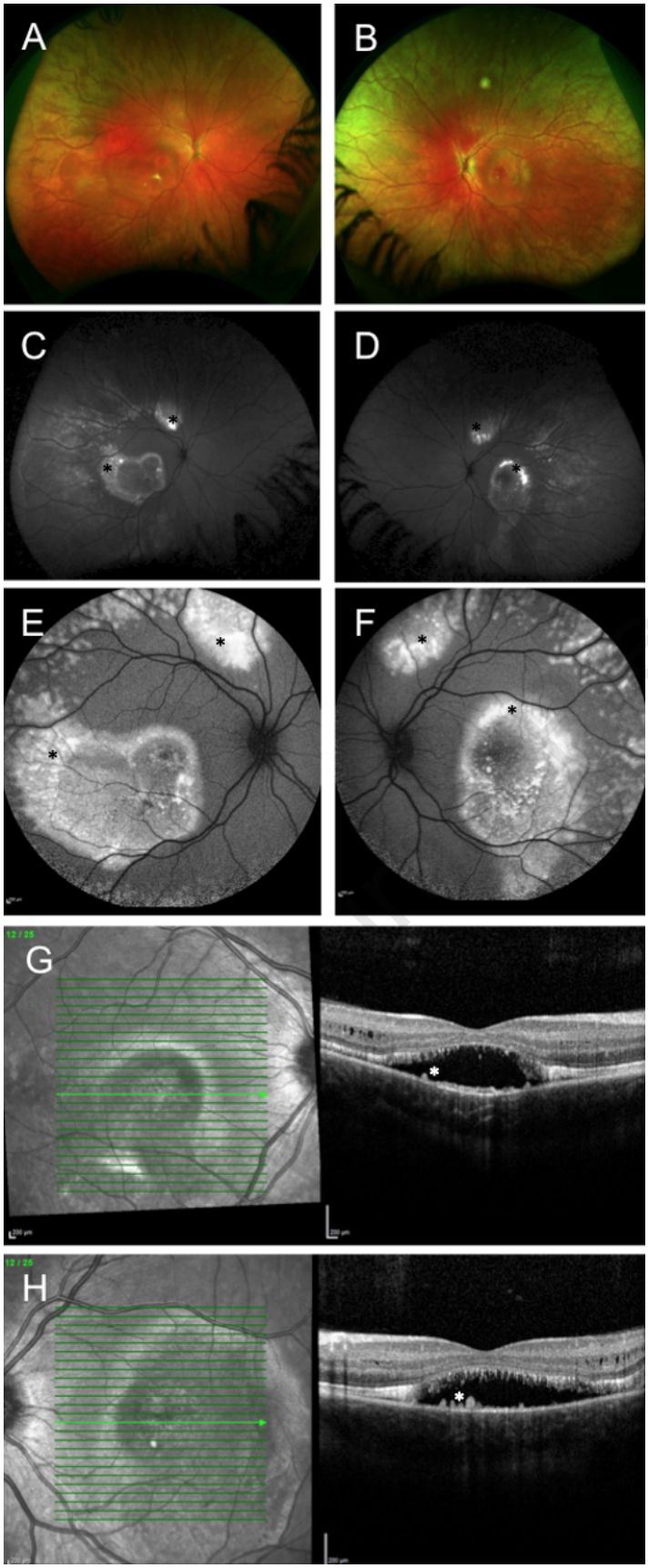

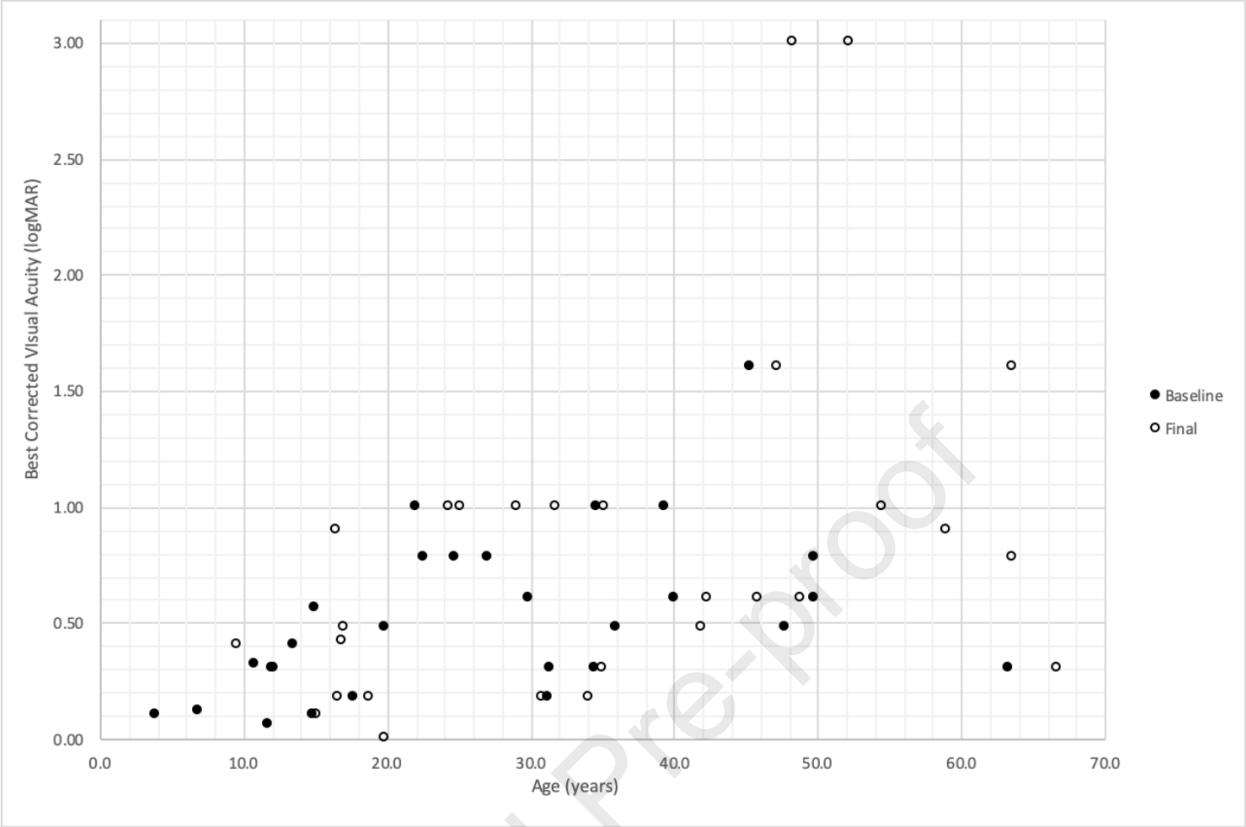

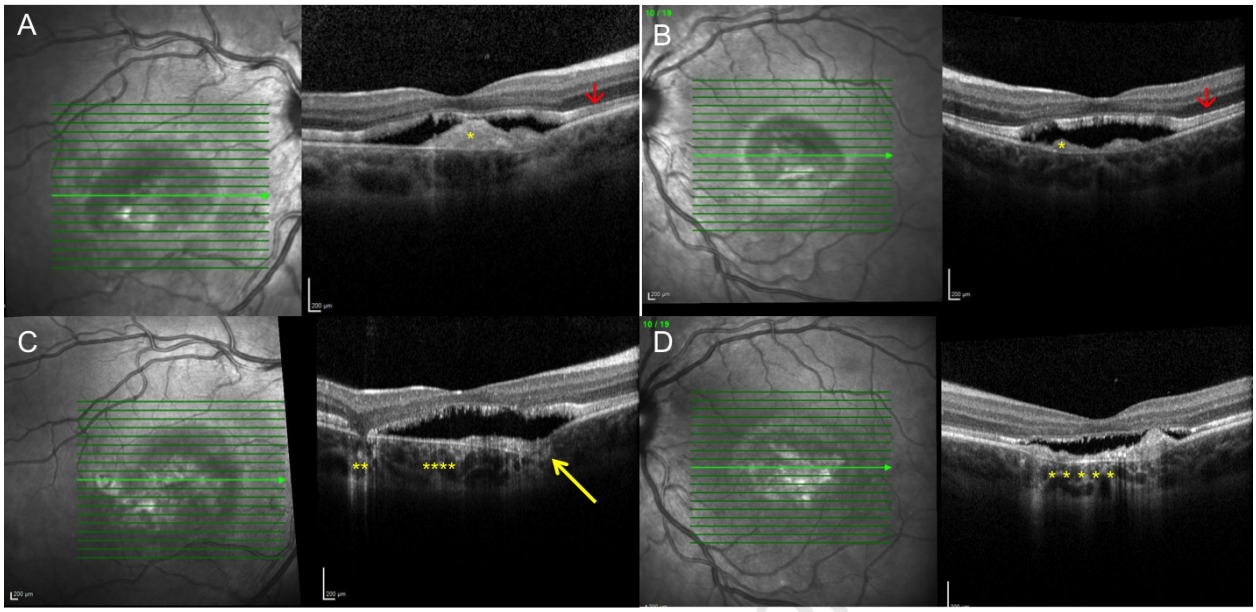

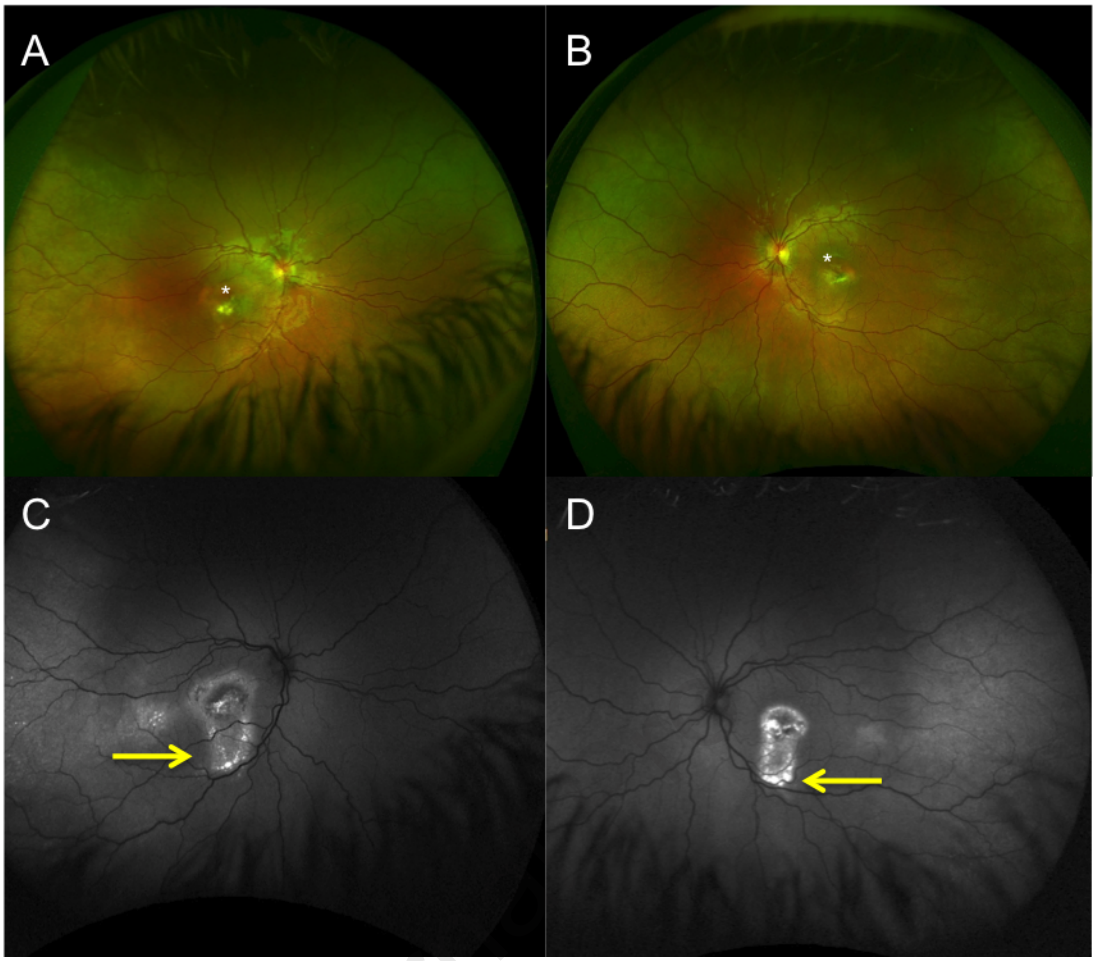

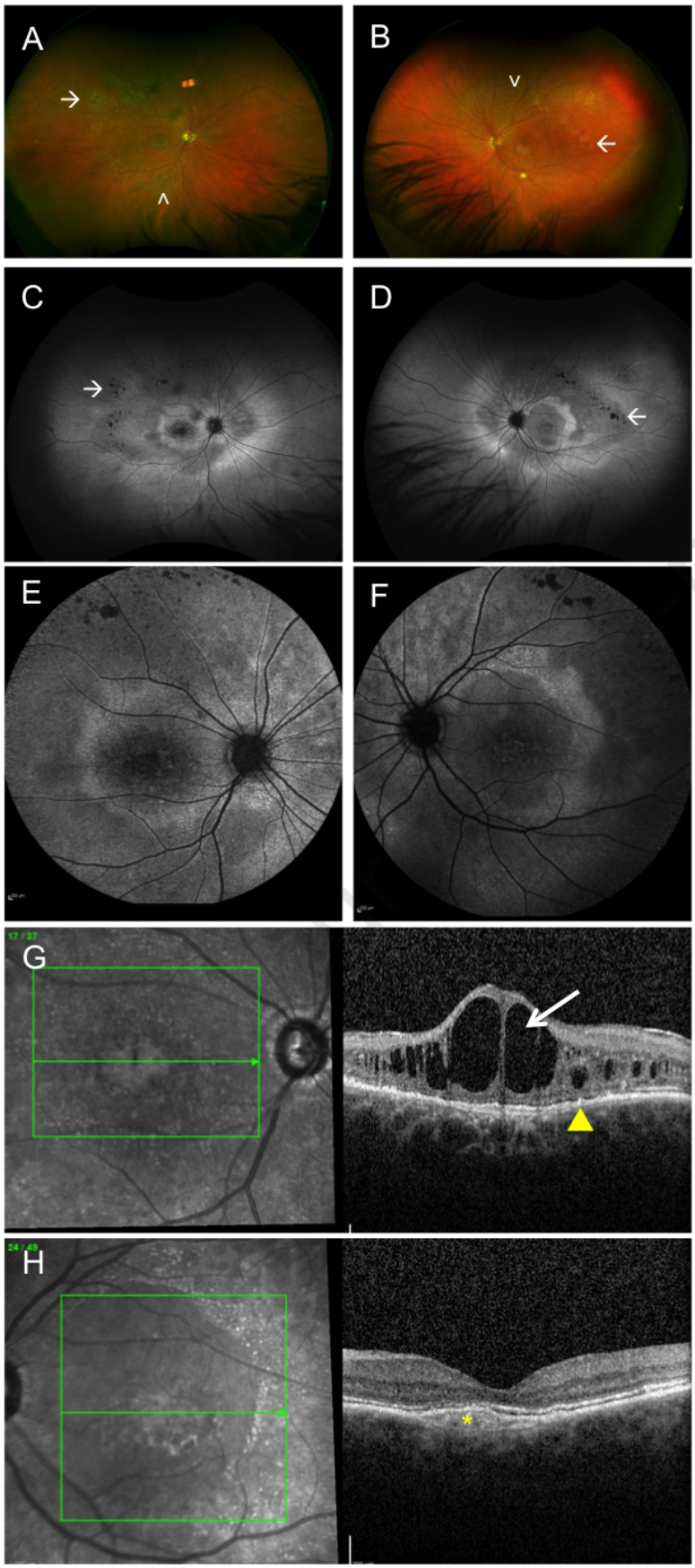

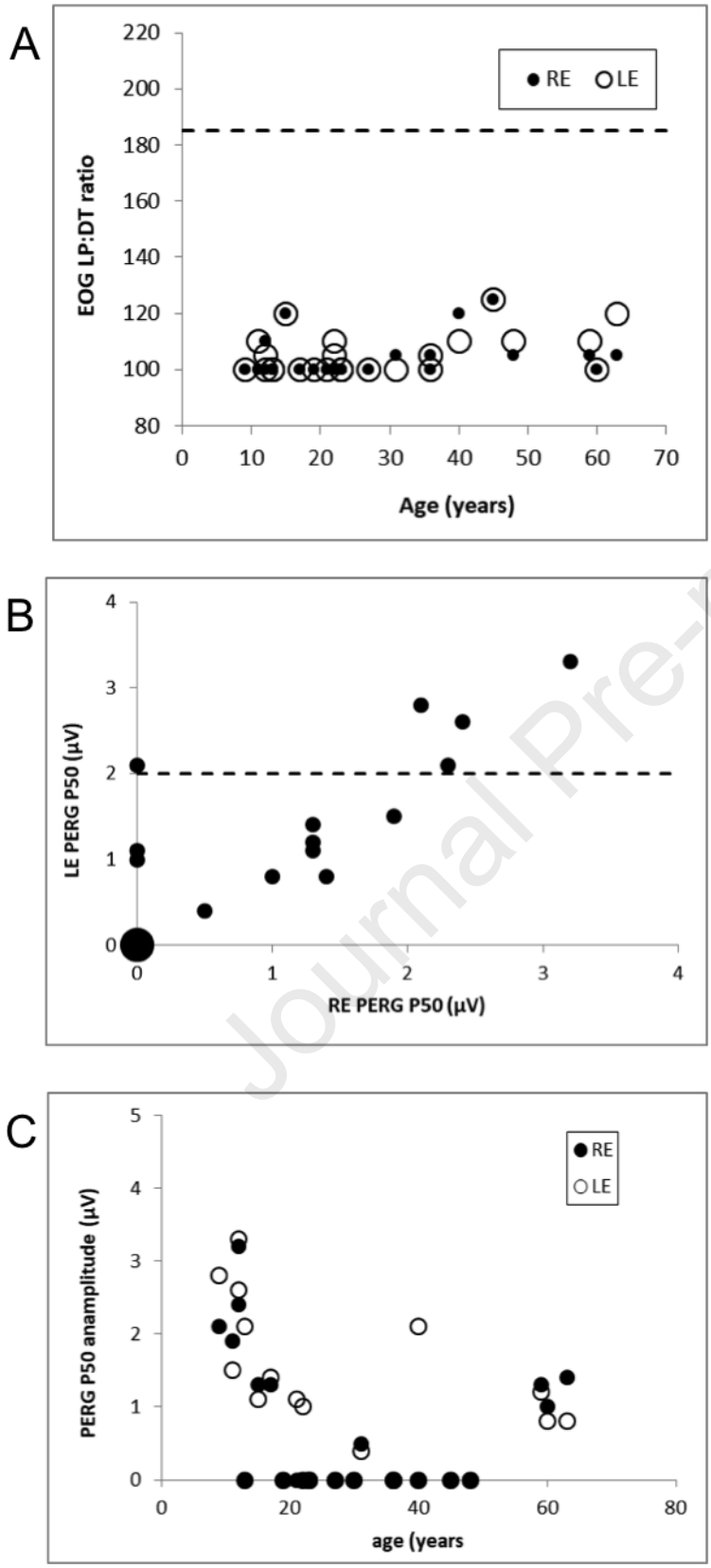

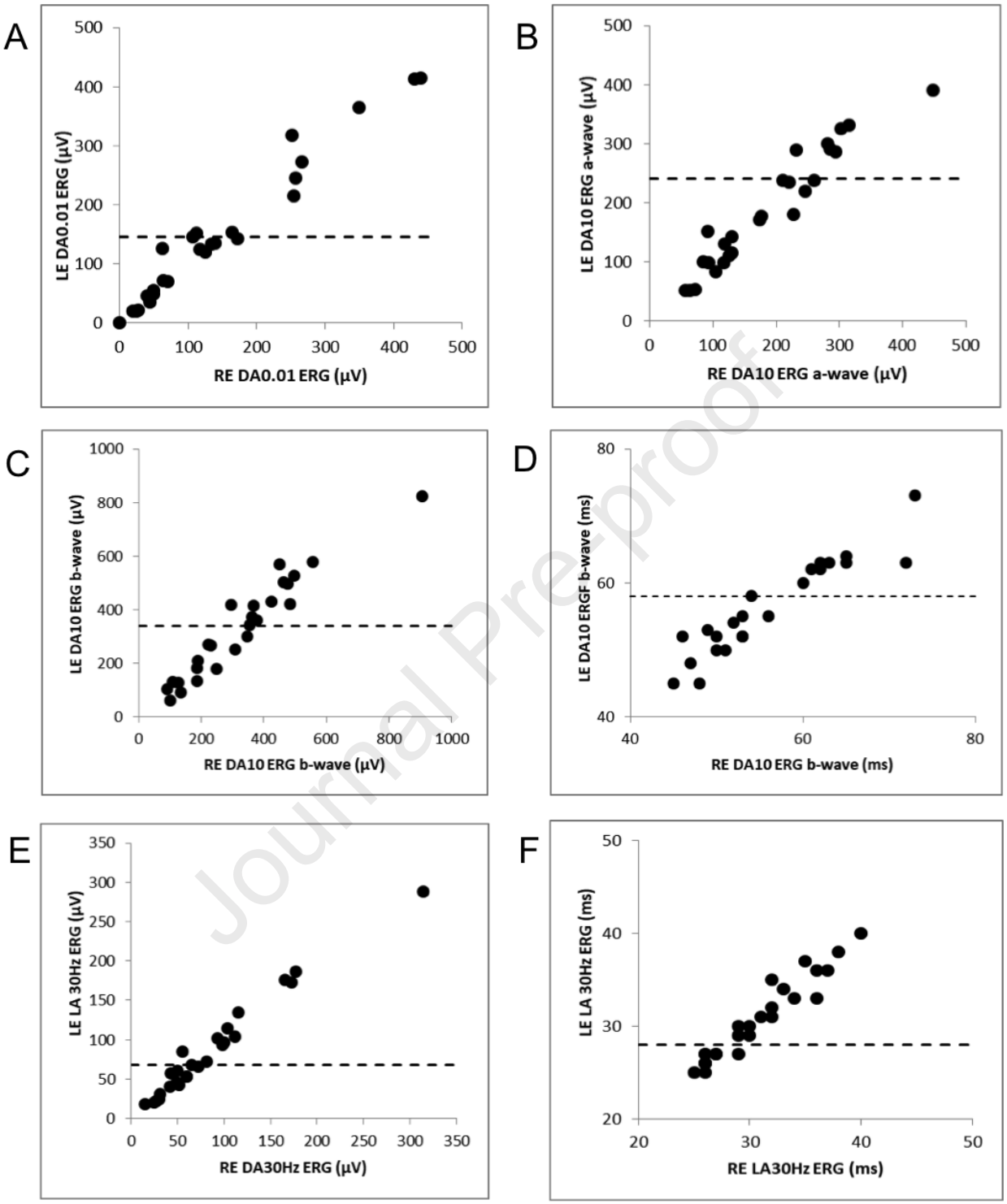

A

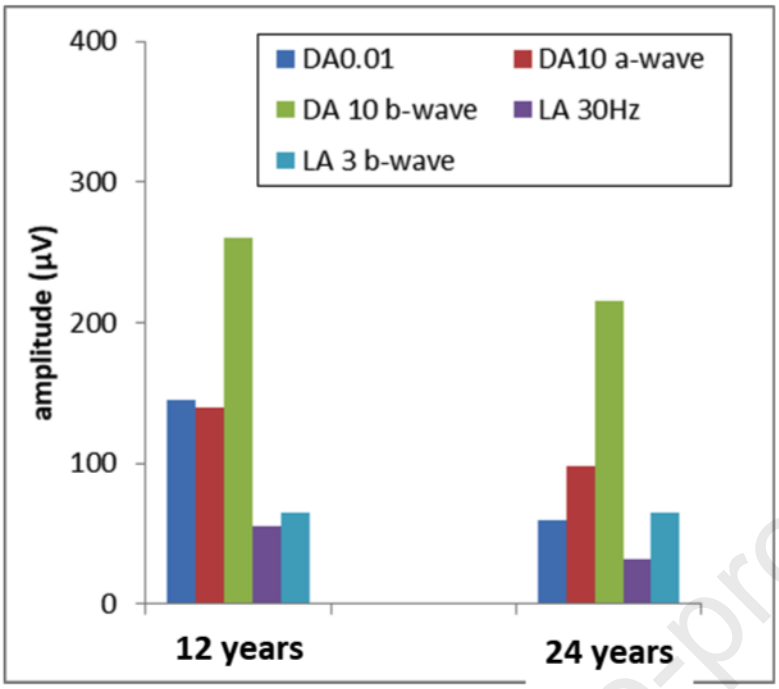

B

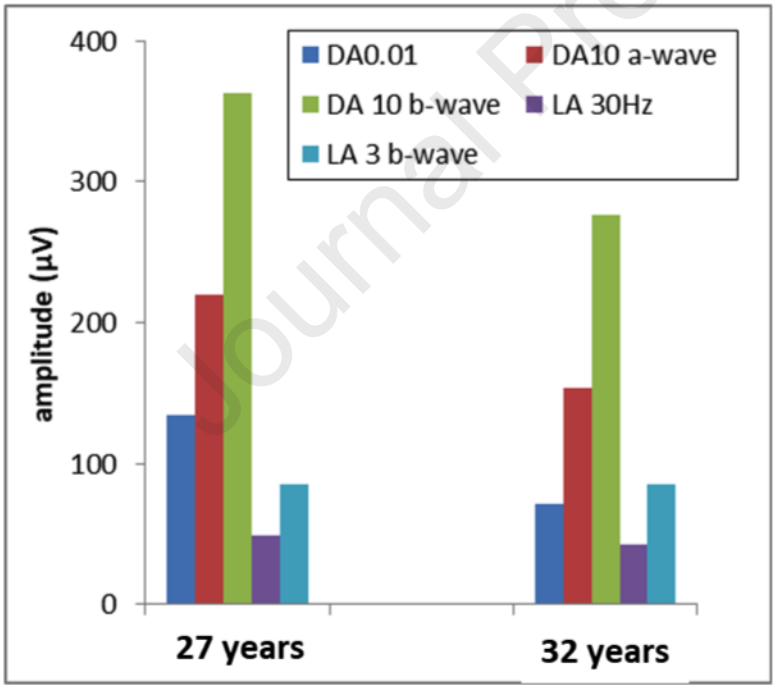

Herein, we present clinical, imaging, electrophysiologic and molecular features from the largest series of ARB patients reported to date. This will better inform patient counselling and contribute to the design of anticipated interventional studies.